Supporting Information for

A structurally precise mechanism links an epilepsy-associated KCNC2 potassium channel mutation to interneuron dysfunction

Jerome Clatot, Christopher B. Currin, Qiansheng Liang, Tanadet Pipatpolkai, Shavonne L. Massey, Ingo Helbig, Lucie Delemotte, Tim P. Vogels, Manuel Covarrubias, Ethan M. Goldberg

Ethan M. Goldberg
Email: goldberge@chop.edu

This PDF file includes:

Supporting Information Text

Methods

Plasmid preparation, cell culture and transfection. The human *KCNC2* cDNA (reference sequence NM_139137.4) and the variant *KCNC2* c.374G>A were synthesized and subcloned into a pCMV-IRES-EGFP plasmid. HEK293T cells (ATCC, CRL-3216) were maintained in DMEM supplemented with 10% heat-inactivated fetal calf serum and 1% penicillin/streptomycin and grown at 37°C with 5% CO_2. Cells were transfected with a total of 0.2 µg of either wild-type or variant *KCNC2* using with PolyFect transfection reagent (QIAGEN; Germantown, MD, U.S.A.) according to the manufacturer's instructions. Cells were cultured in a 35 mm dish. Twenty-four hours after transfection, cells were trypsinized and seeded to a density that enabled single cells to be identified. GFP-positive cells were chosen for patch-clamp experiments. All recordings and data analysis (below) were performed blind to experimental group.

Whole-cell voltage-clamp electrophysiology in HEK-293 cells. Whole-cell patch clamp biophysical experiments were performed at room temperature using an Axopatch 200B amplifier (Molecular Devices, Sunnyvale, CA) in an extracellular Tyrode's solution consisting of the following: 150 mM NaCl, 2 mM KCl, 1.5 mM $CaCl_2$, 2 mM $MgCl_2$, 10 mM HEPES and 10 mM glucose; pH was adjusted to 7.4 with NaOH. Intracellular solution contained, in mM: 125 KCl, 25 KOH; 1 $CaCl_2$, 2 $MgCl_2$, 4 Na_2-ATP, 10 EGTA, 10 HEPES, with pH adjusted to 7.2 with KOH and osmolarity to 305 mOsm/L with sucrose.

Patch-clamp recordings were carried out in the whole-cell configuration at room temperature. Ionic currents were recorded with an Axopatch 200B amplifier (Axon Instruments, San Jose, CA, U.S.A). Patch pipettes were fashioned from thin-walled borosilicate glass (Harvard apparatus, Holliston, MA, U.S.A.) and fire-polished (Zeitz) to a resistance of 1.7–2.5 MΩ in the whole cell configuration. Voltage errors were reduced via series resistance compensation. Currents were filtered at 5 kHz by a low-pass Bessel filter and digitized at 30 kHz. Data were acquired with pClamp 11 and analyzed with Clampfit (Molecular Devices, Sunnyvale, CA). Transient potassium currents were measured by performing 100 ms step depolarizations to -65 to +45 mV in increments of 5 mV from a holding potential of −120 mV, and the current-voltage relation was constructed. Potassium conductance was determined using the equation: $g_K = I_K/(V - E_K)$ where I_K is the potassium current, V is the membrane potential, and E_K is the calculated reversal potential for potassium. Potassium conductance was then normalized, plotted against voltage and fit with a Boltzmann function to determine $V_{1/2}$ of activation. Deactivation kinetics of tail currents were measured by performing a deactivation protocol consisting of a 40 ms prepulse to +40 mV from a holding potential of -100 mV followed by a repolarization step of 100 ms from potentials between -80 mV to +30 mV in an increment of 5 mV. The time constants (τ) of activation and deactivation were determined via a single exponential fit to the data using Clampfit.

Two-electrode voltage clamp electrophysiology in *Xenopus* oocytes. *Xenopus laevis* surgeries were performed according to a protocol approved by the Institutional Animal Care and Use Committee (IACUC) at The Thomas Jefferson University. As previously described (1), a standard

collagenase-based dissociation technique was used to harvest mature oocytes suitable for heterologous expression and electrophysiological recording. Ovaries were digested with collagenase A in calcium-free ND96 (in mM: NaCl, 96; KCl, 2; $MgCl_2$, 1; HEPES, 5; sodium pyruvate, 2.5; adjusted to pH 7.4 with NaOH) for 1.5 hours. To improve yield, this step was repeated once with fresh collagenase A. Upon completion of the dissociation steps, the oocytes were washed at least 3 times with regular ND-96 including 1.8 mM $CaCl_2$, and at least 3 times additionally with Leibovitz's L-15 medium (500 mL Leibovitz's L-15 medium plus 220 mL H_2O, supplemented with 10 mM HEPES and 0.01 mg/mL gentamicin, and titrated with NaOH to a pH of 7.4). Isolated oocytes were then transferred to a 19 °C incubator and maintained in 35 mm Petri dishes containing Leibovitz's L-15. Mature oocytes lacking the follicular layer of cells (stage V-VI) were then selected for mRNA injection with a nanoliter microinjector using 3-000-203-G/X glass needles (Drummond Scientific). Typically, 46-92 nL of mRNA were injected per oocyte. The mRNA concentration was adjusted to obtain expression levels that are appropriate for TEVC (e.g., 2-7 mA at +50 mV; see below). Injected oocytes were maintained at 19 °C in Leiboitz's L-15 medium until they were transferred to the TEVC chamber for the recording of the expressed currents 24-72 h post-injection.

Oocytes were transferred to a recording chamber containing ND-96 (RC-3Z; Warner Instruments) and whole-oocyte currents were recorded at room temperature (21–23°C) under two-electrode voltage-clamp (TEVC) conditions (OC-725C, Warner Instrument, Hamden, CT) according to established procedures (1). The electrodes were filled with 3 M KCl and all recordings were conducted with ND-96 in the bath. Data acquisition was performed using the

Digidata 1440A and pClamp 10.3 (Molecular Devices, Sunnyvale, CA). Passive leak and capacitance transients were subtracted on-line by means of a standard P/4 protocol.

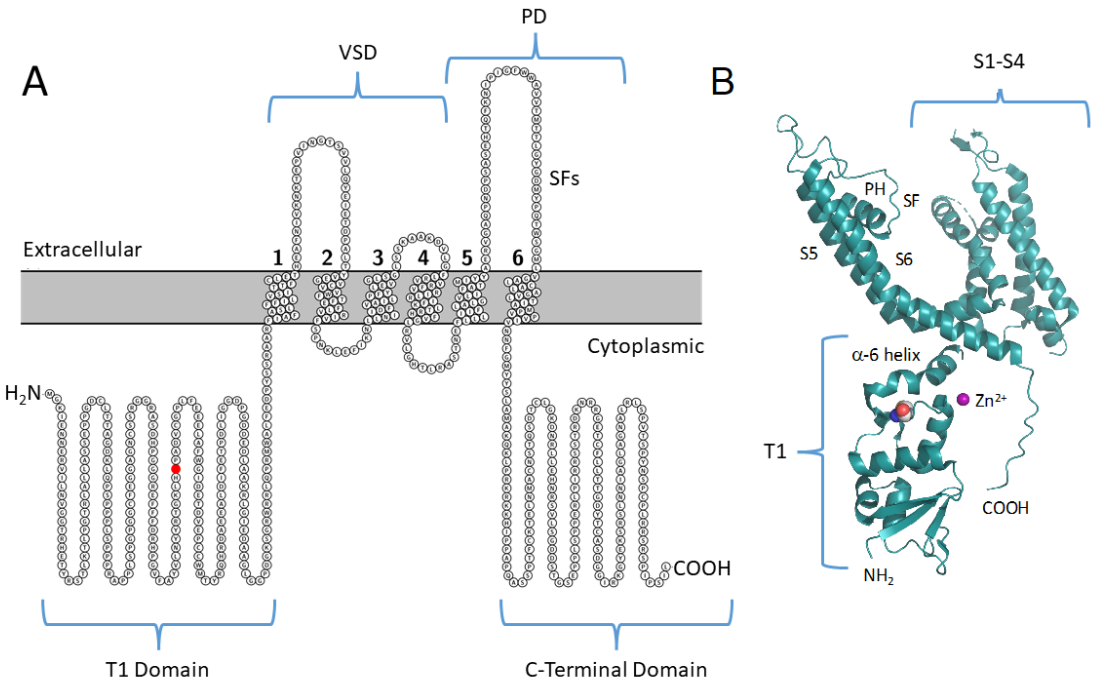

Fig. S1. Topology of the Kv3.2 pore-forming subunit and localization of Cys125. (*A*) Protter-generated topology map of Kv3.2 (2). The red circle in the cytoplasmic T1 domain indicates the location of Cys125. VSD = Voltage Sensing Domain; PD = Pore Domain; SF = Selectivity Filter. The membrane spanning segments S1-S6 are marked by the corresponding numbers. (*B*) 3D model of the Kv3.2 subunit derived from the cryo-EM structure of Kv3.1a. Sphere representations indicate the location of Cys125 and a Zn^{++} atom in the T1 domain. Note that Cys125 is near the α-6 helix of the T1 domain. PH = Pore Helix.

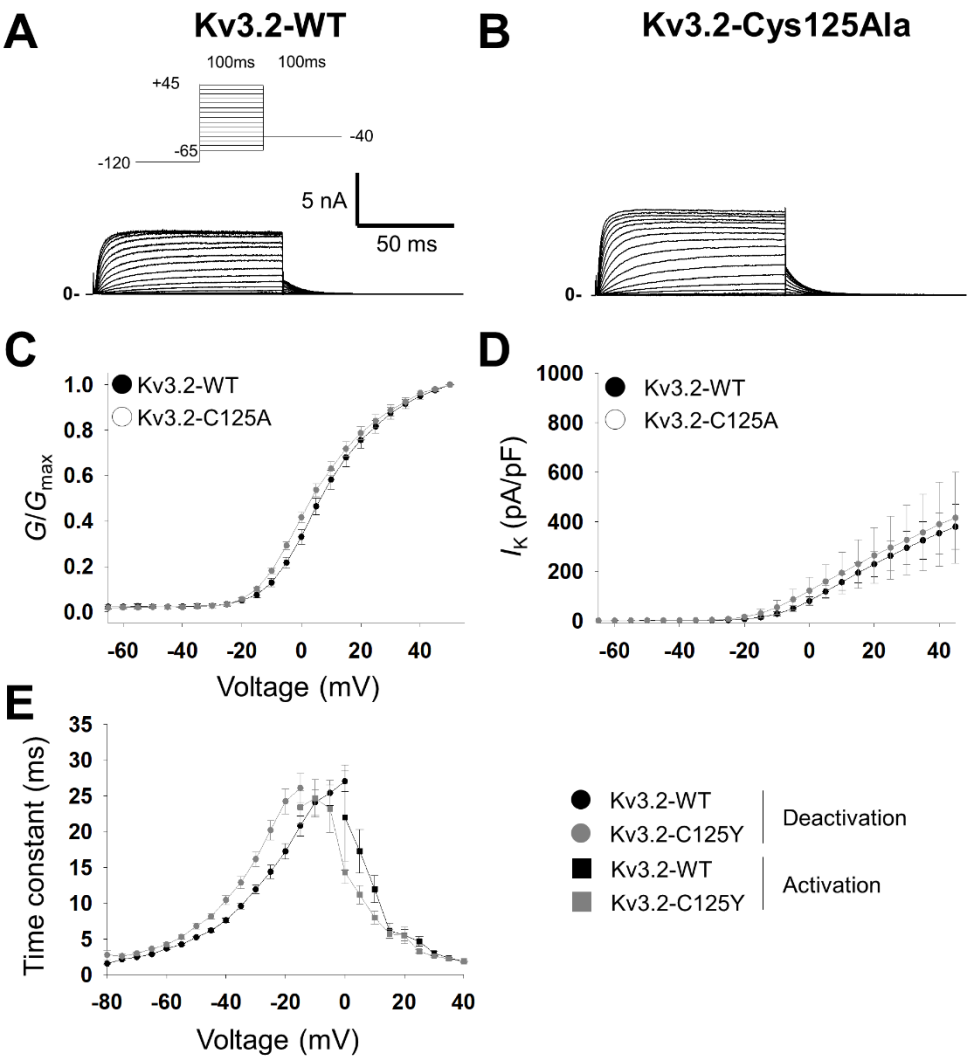

Fig. S2. Electrophysiological properties of Kv3.2-Cys125Ala versus wild-type Kv3.2 in a heterologous system. (*A*) Representative traces for wild-type Kv3.2 and (*B*) Kv3.2-Cys125Ala. (C) There is a small leftward (hyperpolarized) shift in the conductance-voltage (G/G_{max}) curve for Kv3.2-Cys125Ala compared to WT. (*D*) Plot of current density (in pA/pF) versus voltage illustrates normal current density of Kv3.2-Cys125Ala relative to WT. (*D*) Summary data showing accelerated activation and slowed deactivation for Kv3.2-Cys125Ala relative to WT. Circles indicate deactivation, while squares indicate activation; closes black symbols indicate WT, while

closed gray symbols indicate Kv3.2-Cys125Ala. Data is from *n* = 10-12 cells per genotype from *N* = 3 or more separate transfections.

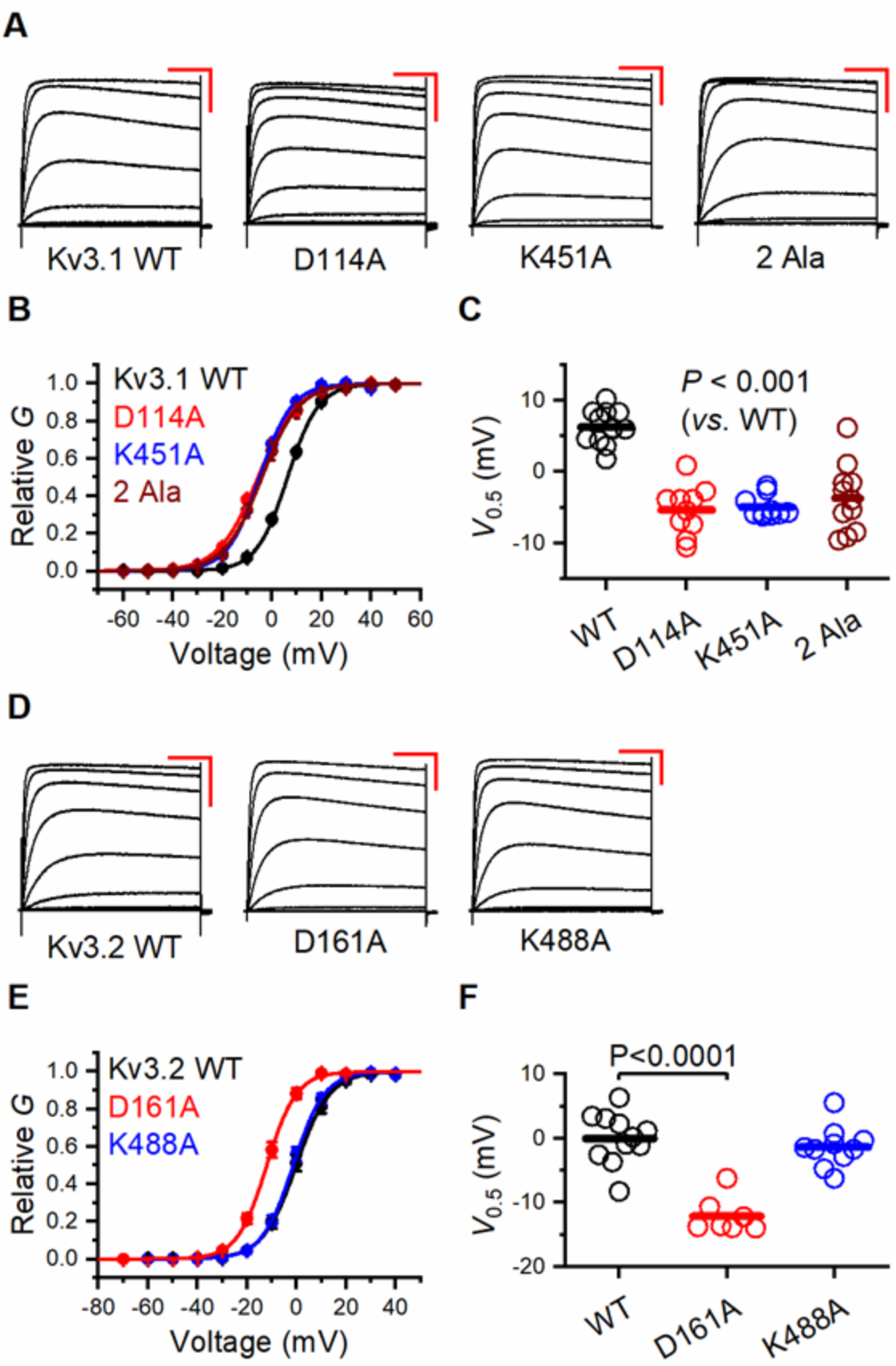
A
Kv3.1 WT
D114A
K451A
2 Ala
B
Kv3.1 WT
D114A
K451A
2 Ala
Relative G
1.0
0.8
0.6
0.4
0.2
0.0
-60 -40 -20 0 20 40 60
Voltage (mV)
C
P < 0.001
(vs. WT)
$V_{0.5}$ (mV)
10
0
-10
WT
D114A
K451A
2 Ala
D
Kv3.2 WT
D161A
K488A
E
Kv3.2 WT
D161A
K488A
Relative G
1.0
0.8
0.6
0.4
0.2
0.0
-80 -60 -40 -20 0 20 40
Voltage (mV)
F
P<0.0001
$V_{0.5}$ (mV)
10
0
-10
-20
WT
D161A
K488A

Fig. S3. Voltage dependent gating and kinetics of Kv3.1 variants Asp114Ala, Lys451Ala, and Asp114Ala + Lys451Ala (2 Ala) and Kv3.2 variants Asp161Ala and Lys488Ala. (*A*) Families of whole-oocyte currents of Kv3.1 wild type (WT), Asp114Ala (D114A), Lys451Ala (K451A), and Asp114Ala + Lys451Ala (D114A + K451A) (2 Ala). Currents were evoked by step depolarizations from a holding voltage of −100 mV. The steps were delivered at 10-second intervals in increments of 10 mV. The scale bars are 100 ms and 1 μA, respectively. (*B*) Normalized peak *G*-*V* relations of the indicated Kv3.1 variants. The solid lines represent best-fit first-order Boltzmann functions. (*C*) Scatter plots of the mid-point voltage ($V_{1/2}$) determined from the peak *G*-*V* relations for the indicated Kv3.1 variants. The horizontal line indicates the mean value. (*D*) Families of whole-oocyte currents of Kv3.2-WT, Kv3.2-Asp161Ala, and Kv3.2-Lys488Ala. (*E*) Normalized peak *G*-*V* relations of the indicated Kv3.2 variants. The solid lines represent best-fit first-order Boltzmann functions. (*F*) Scatter plots of the mid-point voltage ($V_{1/2}$) determined from the peak *G*-*V* relations for the indicated Kv3.2 variants. The horizontal line indicates the mean value.

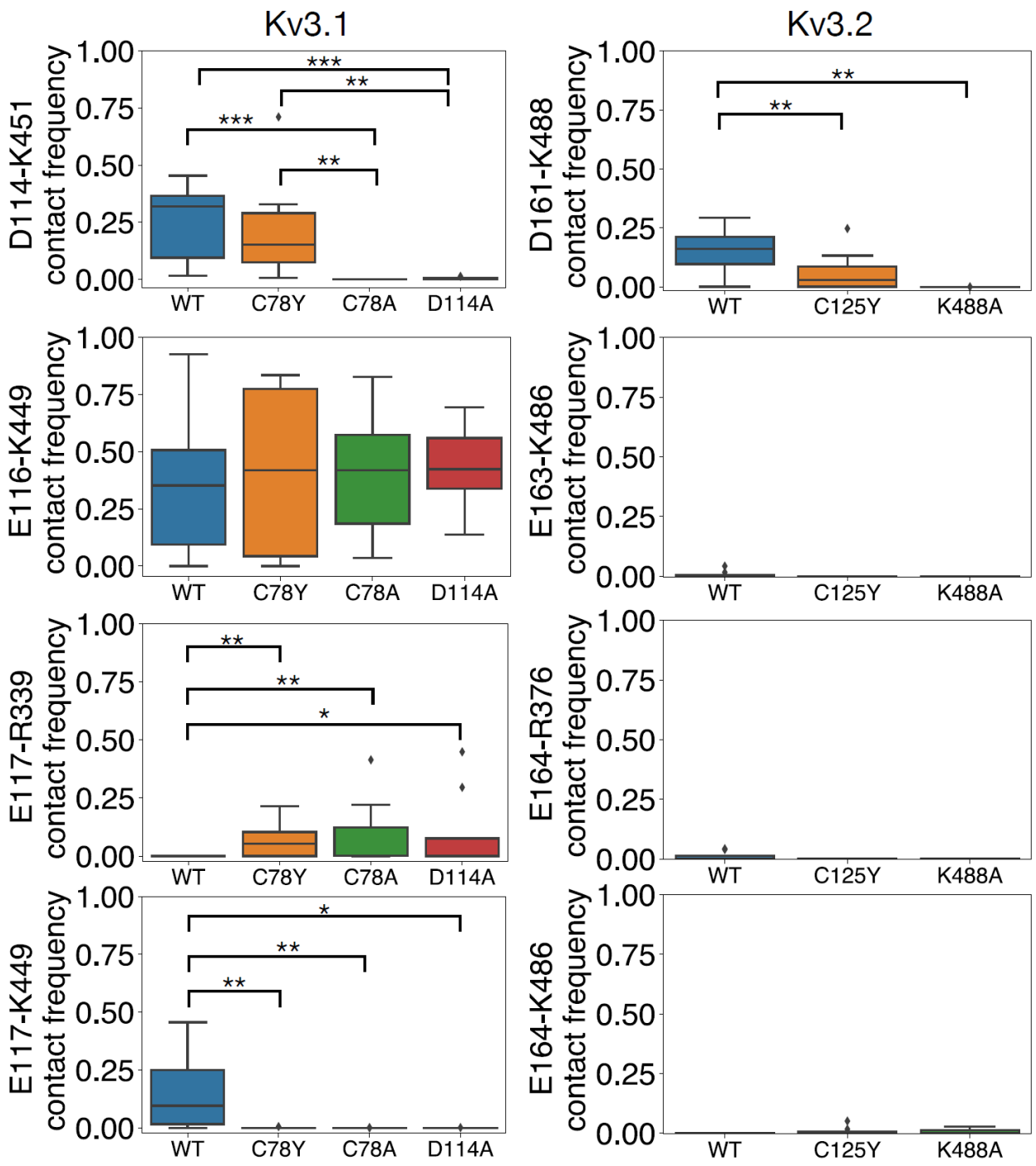

Fig S4. Box plot representation of salt-bridge formation between the alpha-6 helix and the S4-S5 linker and the S6 helix on the Kv3.1, Kv3.2 structures during 700 ns MD simulation. The fractions of frames where two residues denoted on the y-axis are within 4 Å proximity to each other on

Kv3.1 or Kv3.2 over the last 500 ns of the simulation (n = 8). The box represents the interquartile range (IQR) and the whisker shows the range of data within 1.5x of the IQR. Data beyond 1.5x of the IQR is shown as the diamond. All data were collected on the last 500 ns of the simulations. *, $p < 0.05$; **, $p < 0.01$; ***, $p < 0.001$; via Mann Whitney U test.

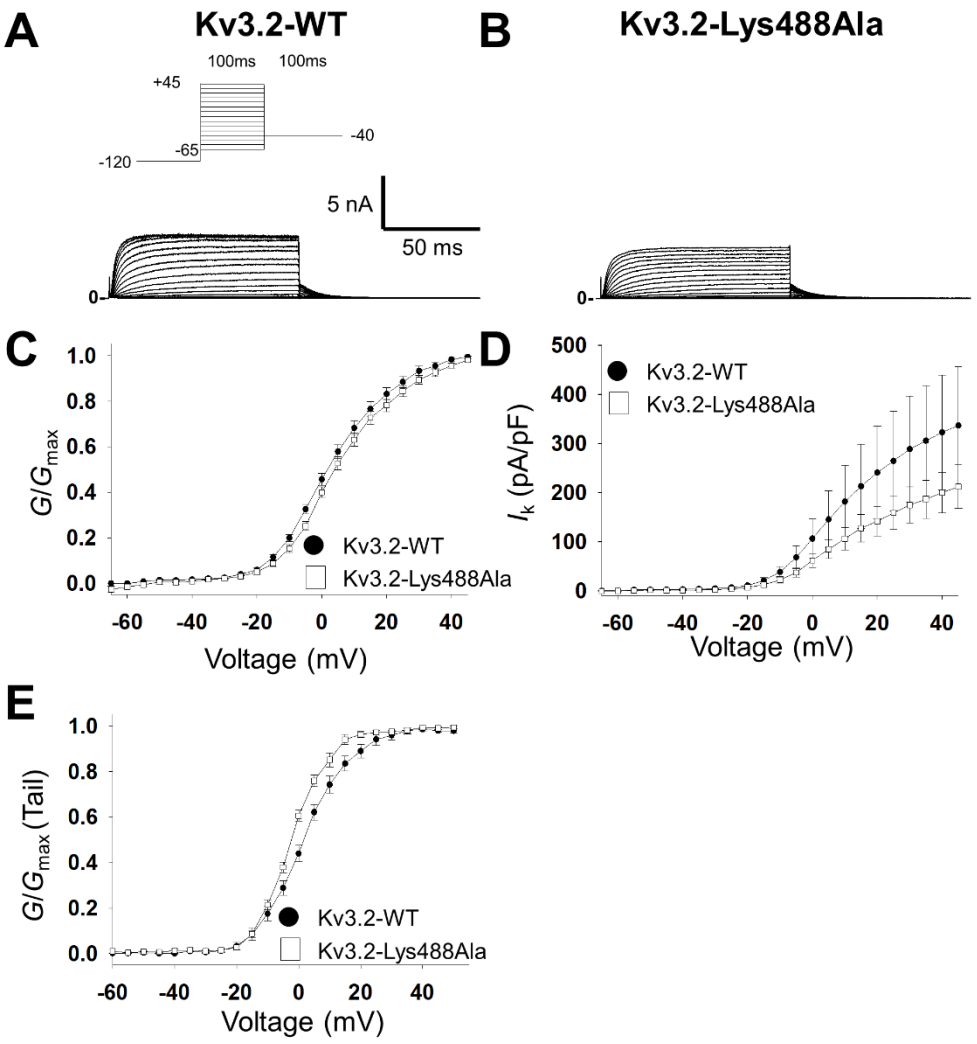

Fig. S5. Electrophysiological properties of Kv3.2-Lys488Ala versus wild-type Kv3.2 in a heterologous system. (*A*) Representative traces for wild-type (Kv3.2-WT) and (*B*) Kv3.2-Lys488Ala. (C) Conductance-voltage (G/G_{max}) curve for WT and Kv3.2-Lys488Ala. (*D*) Plot of current density (in pA/pF) versus voltage illustrates normal current density of Kv3.2-Lys488Ala relative to WT. (*E*) G/G_{max} curve for the tail currents for WT and Kv3.2-Lys488Ala demonstrating a small left shift in the voltage dependence for Kv3.2-Lys488Ala relative to WT.

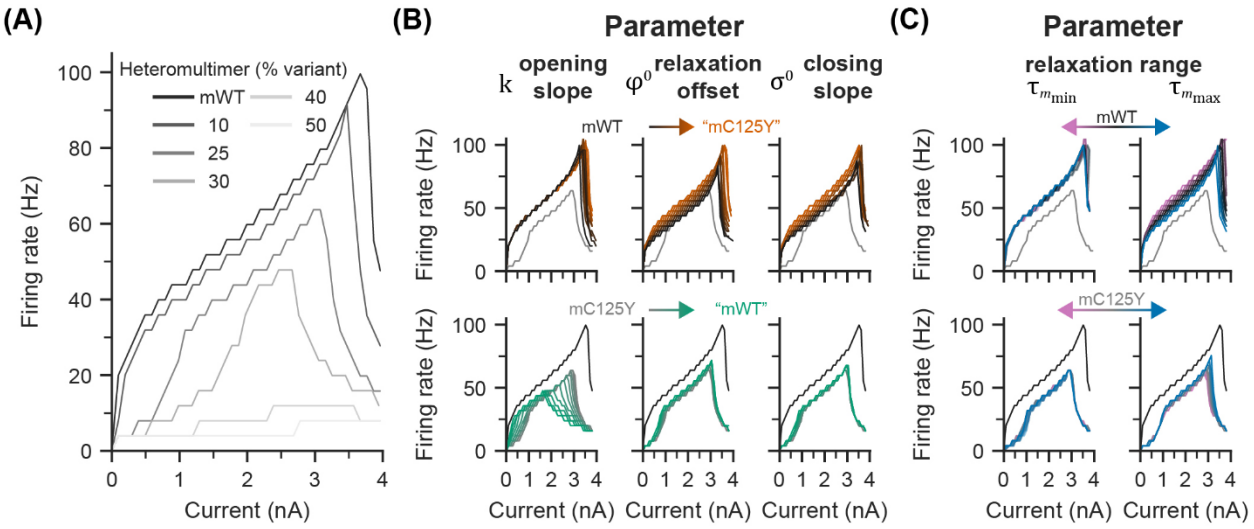

Fig. S6. Manipulation of additional biophysical parameters in the PV-IN model. (*A*) Frequency-current (F-I) curves for heteromultimers of mWT and the mCys125Tyr variant along intermediate values from mWT to 50% mCys125Tyr (*greyscale*). (*B*) The top row shows the change in various parameters of the mWT for it to be more like the mCys125Tyr variant (*orange*) and the bottom row represents adjusting a parameter in the mCys125Tyr variant to be more like mWT. (*C*) Parameter exploration for values that were the same in both mWT and mCys125Tyr variant, namely τ_{min} and τ_{max}. Values were evenly adjusted between 80% (pink) and 120% (blue) of their initial value. As before, top row changes the parameter for a PV interneuron with mWT parameters and the bottom row changes the parameter for a PV interneuron with 25% mCys125Tyr variant.

This data supports the conclusion that opening and closing offset are the key biophysical parameters that might lead to impaired PV-IN excitability (see Fig. 5).

Group	Voltage dependence of activation ($V_{1/2}$)	D$V_{1/2}$	*p* (vs. WT)	*p* (vs. C125A)	*n*
	mV	mV			
WT	-0.8 ± 1.2				9
C125A	-4.2 ± 0.7*	-3.4	0.0217		10
C125Y	-30.0 ± 1.1***	-29.3	5.2E-13	4.6E-14	11
WT	-1.4 ± 1.3				10
C125W	-43.8 ± 0.8***	-42.4	5.8E-17		11

Table S1. Biophysical properties of wild-type and variant hKv3.2 in Xenopus oocytes.

* $p < 0.05$; **, $p < 0.01$; ***, $p < 0.001$; vs. WT via one-way ANOVA.

Group	Voltage dependence of activation ($V_{0.5}$; in mV)	$\Delta V_{0.5}$ (in mV)	*p* (vs. WT)	*p* (vs. C78Y)	*n*
Kv3.1-WT	9.2 ± 0.6				13
Cys78Ala	-2.6 ± 1.1	-11.8	1.2E-09		11
Cys78Tyr	-7.2 ± 1.2	-16.4	5.0E-12	8.7E-03	12

Table S2. Biophysical properties of WT and variant hKv3.1 in Xenopus oocytes.

Group	Voltage dependence of activation ($V_{0.5}$; in mV)	$\Delta V_{0.5}$ (in mV)	*p* (vs. WT)	*n*
Kv3.1-WT	6.3 ± 0.7			12
Asp114Ala	-5.3 ± 1.1	-11.6	9.3E-09	10
Lys451Ala	-5.0 ± 0.5	-11.3	4.9E-11	10
2 Ala	-3.7 ± 1.4	-10.0	2.2E-06	11

Table S3. Properties of WT and variant hKv3.1 in Xenopus oocytes.

Group	Voltage dependence of activation ($V_{0.5}$; in mV)	*p* (vs. WT)	*n*
Kv3.2-WT	-0.0 ± 1.2		11
Asp161Ala	-12.1 ± 1.1	< 0.00001	7
Lys488Ala	-1.4 ± 1.0	0.4068	10

Table S4. Biophysical properties of WT and variant hKv3.2 in Xenopus oocytes.

Supplementary Information References

1. E. Yang, L. Zhi, Q. Liang, M. Covarrubias, Electrophysiological Analysis of Voltage-Gated Ion Channel Modulation by General Anesthetics. *Methods Enzymol* **602**, 339–368 (2018).

2. U. Omasits, C. H. Ahrens, S. Müller, B. Wollscheid, Protter: interactive protein feature visualization and integration with experimental proteomic data. *Bioinformatics* **30**, 884–886 (2014).